Central European Journal of Energetic Materials
ISSN 1733-7178; e-ISSN 2353-1843

Cent. Eur. J. Energ. Mater. 2021, *18*(2): 223-244; DOI 10.22211/cejem/139297
Article is available in PDF-format, in colour, at:
https://ipo.lukasiewicz.gov.pl/wydawnictwa/cejem-woluminy/vol-18-nr-2/

Research paper

Experimental Insight into the Catalytic Mechanism of MFe_2O_4 (M = Ni, Zn and Co) on the Thermal Decomposition of TKX-50

Xiaoting Hou[1,2], Ming Zhang[1], Fengqi Zhao[1,*], Yanjing Yang[1], Ting An[1], Hui Li[1], Qing Pan[1], Xiaohong Wang[1], Kun Zhang[1]

[1] *Xi'An Modern Chemistry Research Institute, China*
[2] *Shanxi North Xing'an Chemical Industry Co., Ltd, China*
* *E-mail:* zhaofqi@163.com

Abstract: Synthesized dihydroxylammonium 5,5'-bistetrazole-1,1'-diolate (TKX-50) owes its outstanding application prospects in the field of insensitive solid propellants not only to its high energetic performance but also to its low mechanical sensitivity. Based on the excellent catalytic activity of bimetallic iron oxides for the thermal decomposition of TKX-50, the catalytic mechanism of bimetallic iron oxides ($NiFe_2O_4$, $ZnFe_2O_4$ and $CoFe_2O_4$) for TKX-50 pyrolysis has been explored. For this study, the decomposition process of TKX-50, before and after mixing with the bimetallic iron oxides $NiFe_2O_4$, $ZnFe_2O_4$ and $CoFe_2O_4$ was monitored by *in-situ* FTIR and gas-phase MS-FTIR instruments. Of the different catalysts, $ZnFe_2O_4$ gave the best result for reducing the initial decomposition temperature of TKX-50. Additionally, the activation energy of functional group cleavage of TKX-50, before and after mixing with $ZnFe_2O_4$, was also calculated for mechanism analysis from the results of the *in-situ* FTIR measurements. The results showed that the condensate and the gas-phase decomposition products of TKX-50 remained unchanged after mixing with different catalysts, while the activation energy of tetrazole ring cleavage was significantly reduced. The results of this study will be helpful for the rational design of insensitive solid propellant formulations containing TKX-50, and for understanding the pyrolysis mechanisms of TKX-50 before and after mixing with the efficient catalyst $ZnFe_2O_4$.

Keywords: bimetallic iron oxide, thermal decomposition, TKX-50, catalysis, mechanism

1 Introduction

Synthesizing energetic materials with both high energy and low sensitivity is essential for their application in military and civilian fields [1, 2]. The energetic performance and sensitivity of energetic compounds greatly influence the operational efficiency and survivability of missile weapons [3, 4]. Synthesized dihydroxylammonium 5,5'-bistetrazole-1,1'-diolate (TKX-50) has attracted extensive attention owing to its excellent energetic performance [5-8]:

– theoretical density: 1.918 $g \cdot cm^{-3}$,
– detonation velocity: 9679 $m \cdot s^{-1}$,
– detonation pressure: 42.4 MPa,
– standard formation enthalpy 446.6 $kJ \cdot mol^{-1}$, and
– low mechanical (impact and friction) sensitivity.

Replacing nitroamine explosives, including hexahydro-1,3,5-trinitro-1,3,5-triazine (RDX) and octahydro-1,3,5,7-tetranitro-1,3,5,7-tetrazocine (HMX), with TKX-50 not only improves the energetic performance of solid propellants, but also avoids the potential risks caused by the introduction of these highly sensitive energetic compounds [9-11].

The thermal decomposition mechanism of an energetic component plays an essential role in the combustion performance and mechanism of a solid propellant [12-14]. Consequently, the pyrolysis mechanism of neat TKX-50 during heat treatment has been studied by various experimental and theoretical methods. Huang *et al.* [15] studied the thermal decomposition performance of neat TKX-50 using TG-DSC and FTIR methods, and the critical explosive temperature and kinetic parameters of TKX-50 were calculated. Additionally, the crystal structure transformation and step-by-step thermal decomposition behaviour of neat TKX-50 were studied by *in-situ* XRD and TG-DSC methods, respectively [16]. The results showed that the crystal structure was transformed from that of TKX-50 to the intermediate product diammonium 5,5'-bistetrazole-1,1'-diolate (ABTOX) under thermal stimulation. The results also showed that the thermal stability of neat TKX-50 is close to that of hexanitrohexaazaisowurtzitane (CL-20) [17].

The thermal decomposition behaviour, kinetic parameters and pyrolysis mechanism of neat TKX-50 has been systematically studied [15-20]. However, the effects of combustion catalysts, which have a critical influence

on the thermal decomposition and combustion performance control of solid propellants, on the decomposition process and pyrolysis mechanism of TKX-50 are seldom reported and require urgent exploration. The catalytic performance of MFe_2O_4 (M = Ni, Co and Zn) on the thermal decomposition behaviour of TKX-50 has been studied previously using DSC and TG-DTG methods, and demonstrated that the thermal decomposition peak temperatures and apparent activation energies of TKX-50 are clearly reduced after the addition of bimetallic iron oxides [20]. However, the catalytic mechanism of MFe_2O_4 (M = Ni, Co and Zn) for the thermal decomposition of TKX-50 is still unclear. Therefore, an urgent exploration of the pyrolysis mechanism of TKX-50 before and after mixing with bimetallic iron oxides is required to better understand the combustion mechanism of solid propellants containing TKX-50.

In the present work, three kinds of bimetallic iron oxides ($NiFe_2O_4$, $ZnFe_2O_4$ and $CoFe_2O_4$) were prepared and used for the study of the thermal decomposition of TKX-50. The pyrolysis mechanism of TKX-50, before and after mixing with the as-synthesized bimetallic iron oxides, during heat treatment was studied by *in-situ* FTIR and gas-phase MS-FTIR methods. Additionally, the kinetic parameters of characteristic group cleavage of TKX-50, before and after mixing with the most efficient catalyst $ZnFe_2O_4$, were calculated using the Coats-Redfern method using the results of the *in-situ* FTIR measurements. Based on the above studies, the pyrolysis mechanisms of TKX-50, before and after mixing with $ZnFe_2O_4$, are suggested (Figure 1).

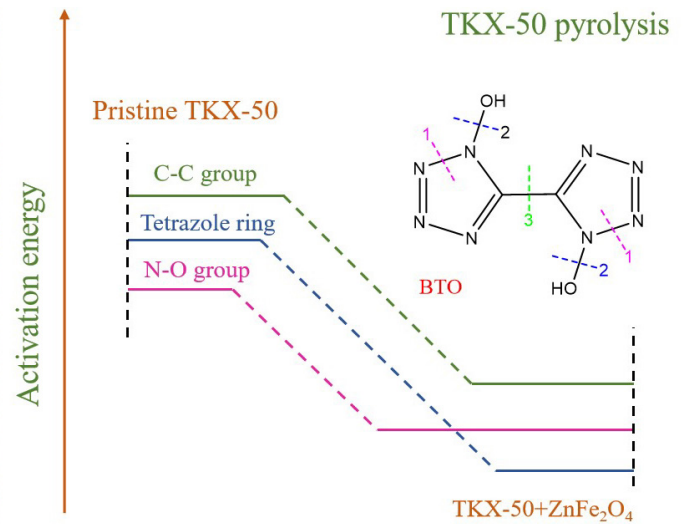

Figure 1. Illustration of the pyrolysis mechanism of TKX-50 before and after mixing with catalysts

2 Experimental

2.1 Materials

All of the chemicals used were analytical grade and used without further purification. Ferric trichloride hexahydrate ($FeCl_3 \cdot 6H_2O$), nickel chloride hexahydrate ($NiCl_2 \cdot 6H_2O$), zinc chloride ($ZnCl_2$), cobalt chloride hexahydrate ($CoCl_2 \cdot 6H_2O$), sodium acetate and polyethylene glycol (M_n = 4000) were purchased from Aladdin Inc. Ethylene glycol (Sinopharm Chemical Reagent Co., Ltd.), ethanol (EA) (Xi'an Chemical Reagent Factory) and distilled water were used for sample preparation and treatment. TKX-50 of purity greater than 99.5% was obtained from Xi'an Modern Chemistry Research Institute.

2.2 Preparation of MFe_2O_4 (M = Ni, Zn and Co)

Calculated quantities of $FeCl_3 \cdot 6H_2O$ (5 mmol) were dissolved and mixed individually with $NiCl_2 \cdot 6H_2O$, $ZnCl_2$ and $CoCl_2 \cdot 6H_2O$ (2.5 mmol) in ethylene glycol (60 mL) under magnetic agitation, respectively. Sodium acetate (3.6 g) and polyethylene glycol (1.0 g) were then added to the above three solutions and mixed thoroughly. The reactants were transferred to a 100 mL Teflon-sealed autoclave and heated at 180 °C for 24 h. After cooling, the products were filtered off and washed several times with distilled water and absolute alcohol, and then cured at 60 °C in a vacuum oven overnight. The powder obtained was ground for further characterization [20, 21]. Fe_2O_3 nanoparticles with an average particle size of 110 nm were prepared according to the published literature [22, 23].

2.3 Characterization

An *in-situ* Fourier transform infrared spectrometer (*in-situ* FT-IR, USA, Thermo-Fisher, NEXUS 870) was used to characterize the decomposition process of TKX-50 before and after mixing with different catalysts, at heating rates of 5, 10, 15 and 20 °C·min^{-1} (air atmosphere, temperature range of 25-465 °C, spectral resolution of 4 cm^{-1}, sweep speed of 7.5 files·min^{-1} and 8 scans·file^{-1}, sample mass of 1.2 mg mixed with 250 mg potassium bromide). The samples (TKX-50 before and after mixing with different bimetallic iron oxides) were characterized using thermogravimetric analysis-differential scanning calorimetry-mass spectrometry-Fourier transform infrared spectroscopy (TG-DSC-MS-FTIR) methods for mechanism analysis (Ar flow rate 50 mL/min, sample mass of 1.0 ±0.2 mg). The gas phase products were analyzed according to the results of MS-FTIR (NETZSCH STA 449C with a TASC 414/4 controller, NETZSCH 403C, NICOLET 5700 and CDS pyroprobe 5600 series).

2.4 Kinetic calculations

The activation energies for characteristic group cleavage of TKX-50, before and after mixing with $ZnFe_2O_4$, were calculated from the results of the *in-situ* FTIR measurements at heating rates of 5, 10, 15 and 20 °C·min^{-1}. The conversion degree (α) of TKX-50 was calculated using Equation 1.

$$\alpha = \frac{Max-X}{Max-Min} \tag{1}$$

where X is the transmittance value at a certain temperature, *Max* and *Min* are the maximum and minimum transmittance values in the thermal decomposition range, respectively. The activation energy of the C–C bond, N–O bond and tetrazole ring cleavage were calculated by the Coats-Redfern method (Equation 2).

$$\ln\frac{g(\alpha)}{T^2} = \ln\left(\frac{AR}{\beta E}\right) - \frac{E}{RT} \tag{2}$$

where $g(\alpha)$ is the mechanism function, E is activation energy, T is temperature, β is heating rate, R is universal gas constant, and A is pre-exponential factor.

3 Results and Discussion

3.1 *In-situ* FT-IR analysis

The FT-IR spectra of TKX-50 before and after mixing with different catalysts at 25 °C are shown in Figure 2(a), and the corresponding absorption peaks are listed in Table 1. As shown in Table 1, the absorption peaks at 3220 and 3084~2500 cm^{-1} can be attributed to the O–H and NH_3^+ stretching vibrations of NH_3OH^+, respectively. The absorption peaks at 1577, 1526 and 1426 cm^{-1} are due to the stretching vibrations of the tetrazole ring. The peaks at 1235 and 716 cm^{-1} are due to the stretching vibrations of the N–O and C–C bonds, respectively. The FT-IR spectra of TKX-50 before and after mixing with different catalysts showed no obvious change, indicating that different catalysts would not affect the FT-IR peaks of TKX-50.

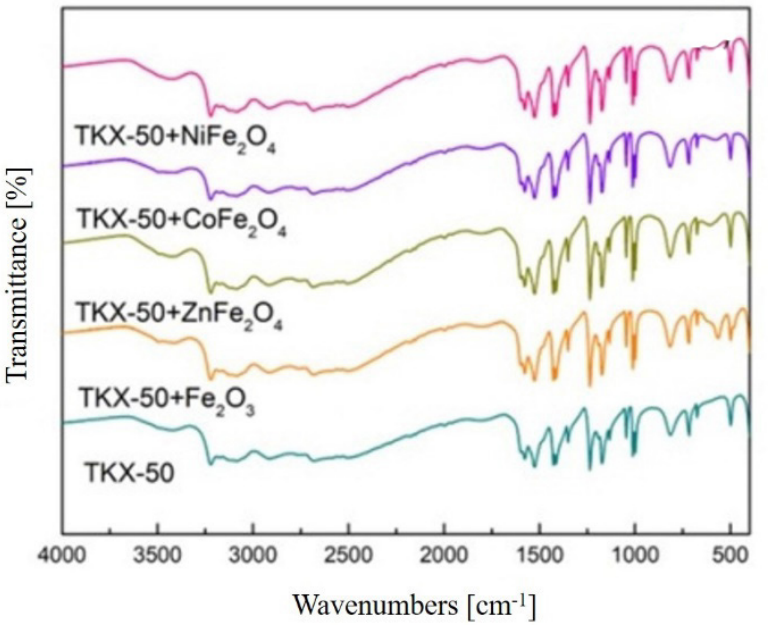

(a)

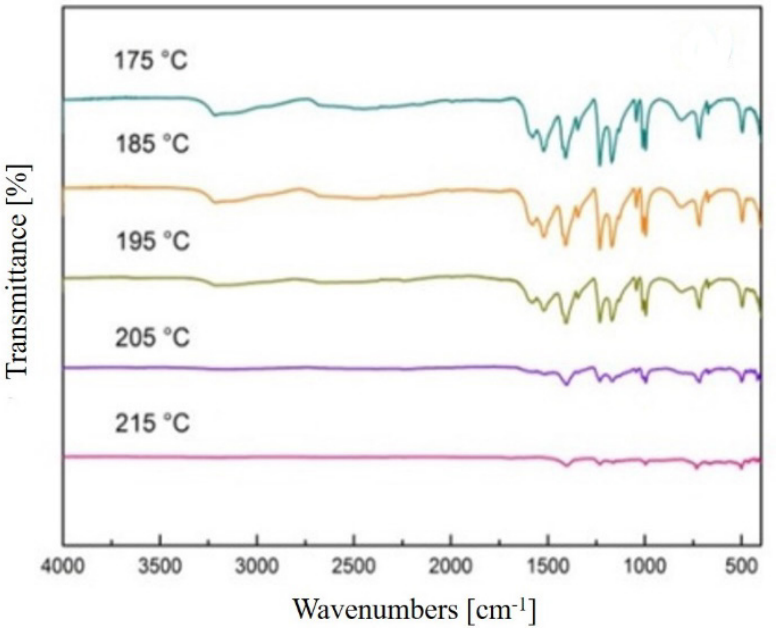

(b)

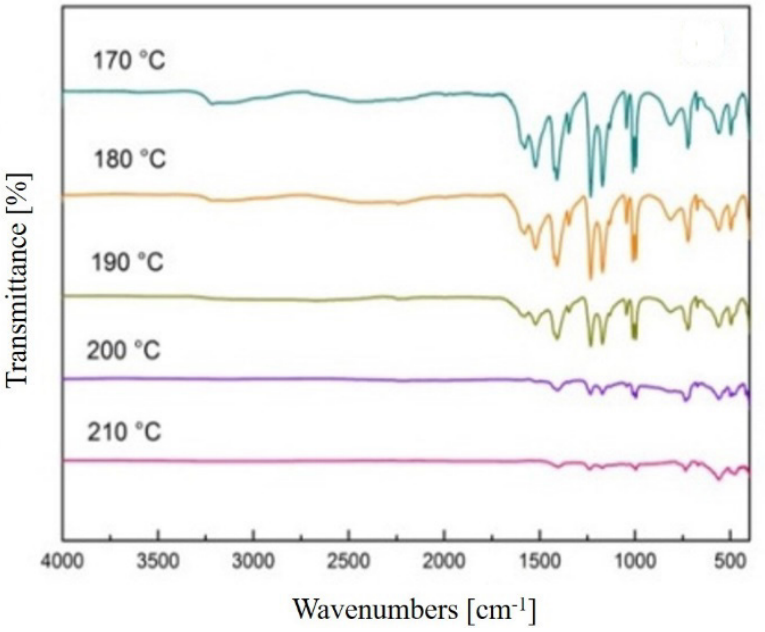

(c)

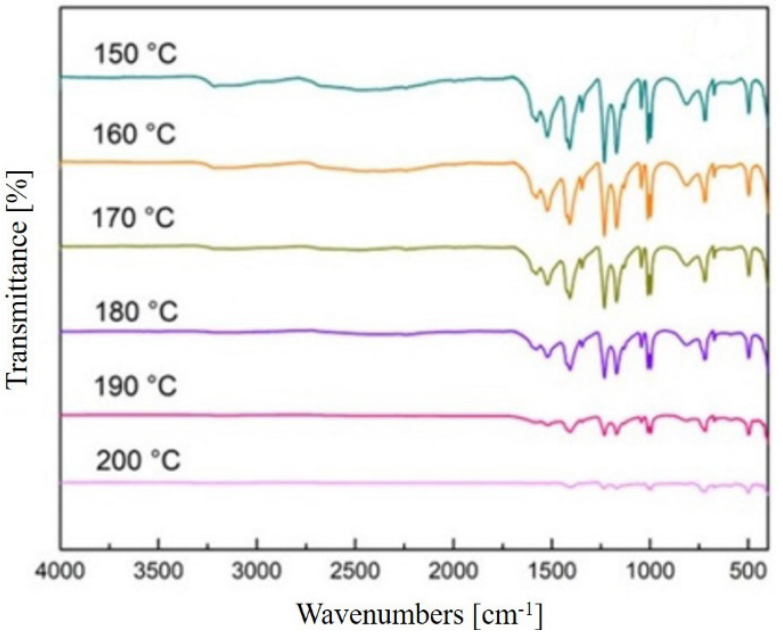

(d)

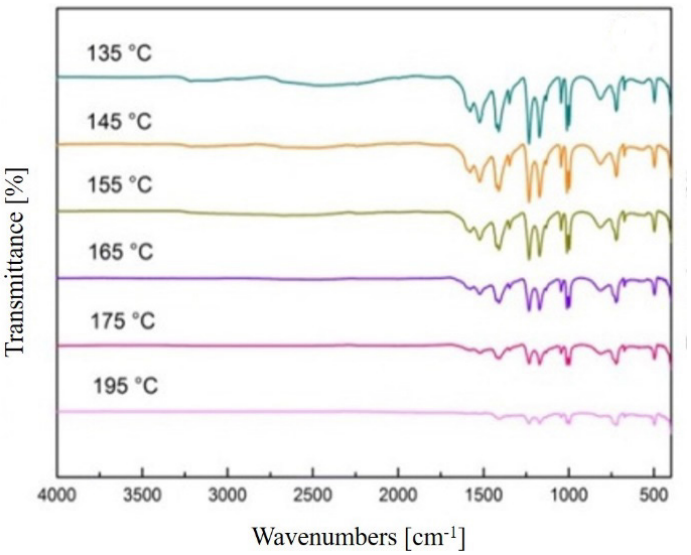

(e)

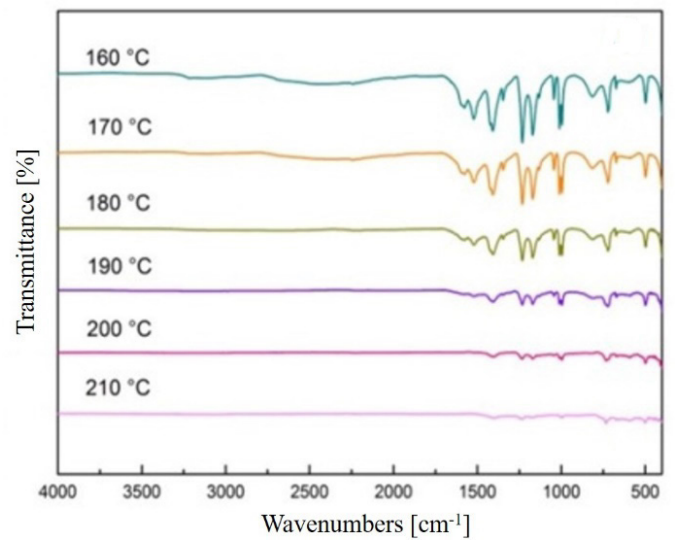

(f)

Figure 2. FTIR spectra of: (a) TKX-50 before and after mixing with different catalysts at 25 °C, (b) neat TKX-50 at 175-215 °C, (c) TKX-50 mixed with Fe_2O_3 at 170-210 °C, (d) TKX-50 mixed with $ZnFe_2O_4$ at 150-200 °C, (e) TKX-50 mixed with $CoFe_2O_4$ at 135-195 °C, and (f) TKX-50 mixed with $NiFe_2O_4$ at 160-210 °C

Table 1. FTIR absorption peaks of the characteristic groups in TKX-50

Wavenumber [cm^{-1}]	Vibration type	Functional group
3220	ν	O–H
3084-2500	ν	NH_3^+
1577, 1526, 1426	ν	Tetrazole ring
1235	ν	N–O
716	ν	C–C
814	ν	N–H

Additionally, the *in-situ* FT-IR images of TKX-50 before and after mixing with different catalysts at 10 °C·min^{-1} were characterized, and the corresponding FT-IR spectra at different temperature are shown in Figures 2(b)-2(f). The *in-situ* FT-IR spectra showed that the intensity of the absorption peaks decreased with an increase in temperature, indicating that TKX-50 decomposes gradually. Additionally, the initial pyrolysis temperature of TKX-50 during heat treatment was decreased after addition of the catalysts. Of the different catalysts, the pyrolysis temperature of TKX-50 + $CoFe_2O_4$ and TKX-50 + $ZnFe_2O_4$ decreased most clearly, which demonstrated the excellent catalytic performance of $CoFe_2O_4$ and $ZnFe_2O_4$. The results are consistent with those from our previous study, that is, $CoFe_2O_4$ and $ZnFe_2O_4$ exhibit excellent performance on reducing the thermal decomposition peak temperatures of TKX-50. The synthesized $ZnFe_2O_4$ has the best effect on the thermal decomposition of TKX-50, and can effectively reduce the thermal decomposition temperature and apparent activation energies of TKX-50 [20].

3.2 Gas-phase MS analysis

The MS curves of the gas-phase TKX-50 thermal decomposition products are shown in Figure 3. This shows that the main decomposition products of TKX-50 are [24]:

– NH_3 (confirmed by the appearance of m/z = 17 and 15),
– H_2O (confirmed by the appearance of m/z = 18),
– HCN (confirmed by the appearance of m/z = 27 and 26),
– N_2 or CO (confirmed by the appearance of m/z = 28),
– NO (confirmed by the appearance of m/z = 30),
– CO_2 or N_2O (confirmed by the appearance of m/z = 44), and
– NO_2 (confirmed by the appearance of m/z = 46).

After the addition of a bimetallic iron oxide ($NiFe_2O_4$, $ZnFe_2O_4$ and $CoFe_2O_4$), the pyrolysis products of TKX-50 thermal decomposition showed no obvious differences. However, the peak temperature for ion production was quite different,

which indicates the catalytic effects of MFe_2O_4 for the thermal decomposition of TKX-50. Additionally, the variation trend for the peak temperature was in good agreement with the results of the *in-situ* FTIR measurements, which also confirms the excellent catalytic activity of $CoFe_2O_4$ and $ZnFe_2O_4$ for TKX-50 thermal decomposition.

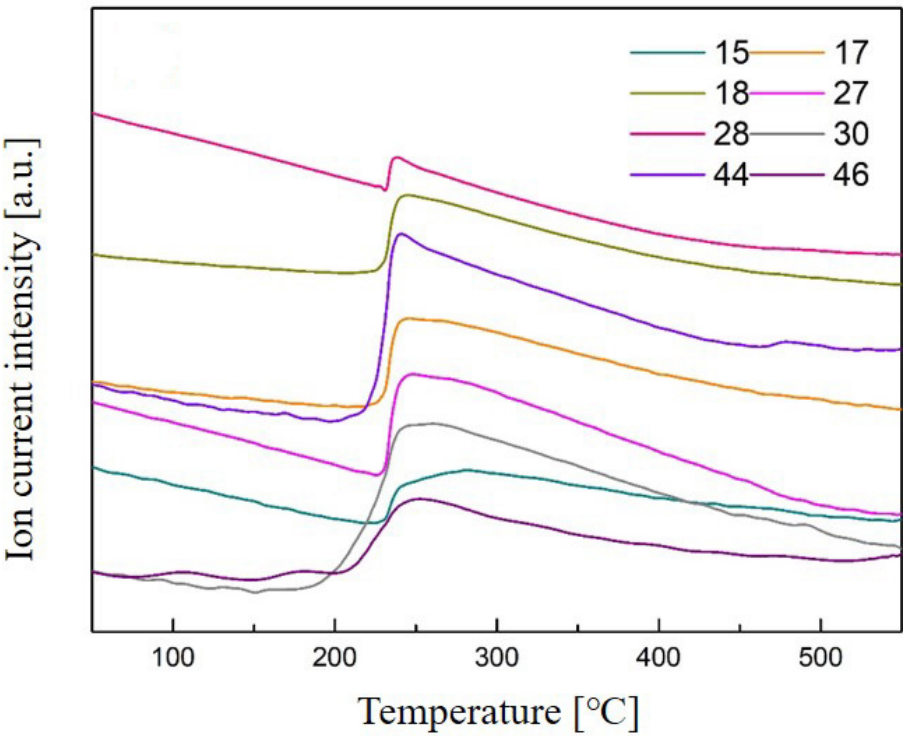

(a)

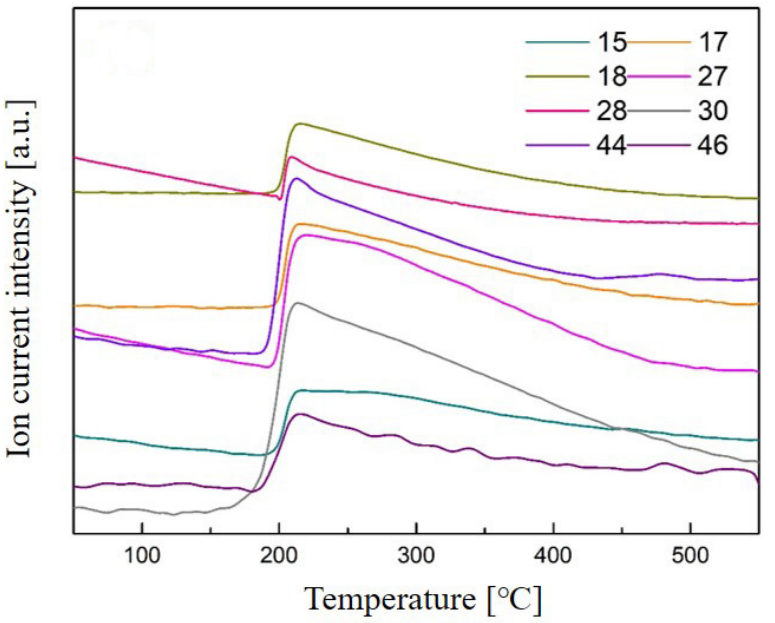

(b)

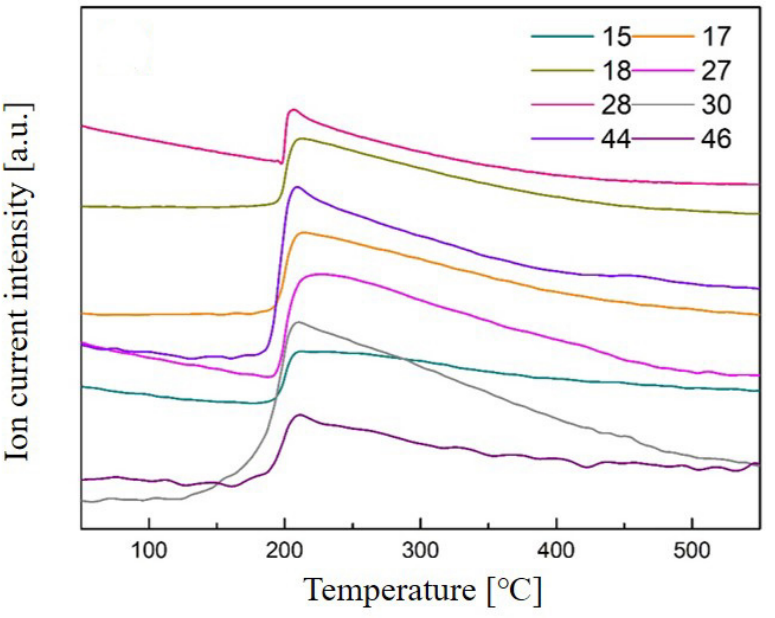

(c)

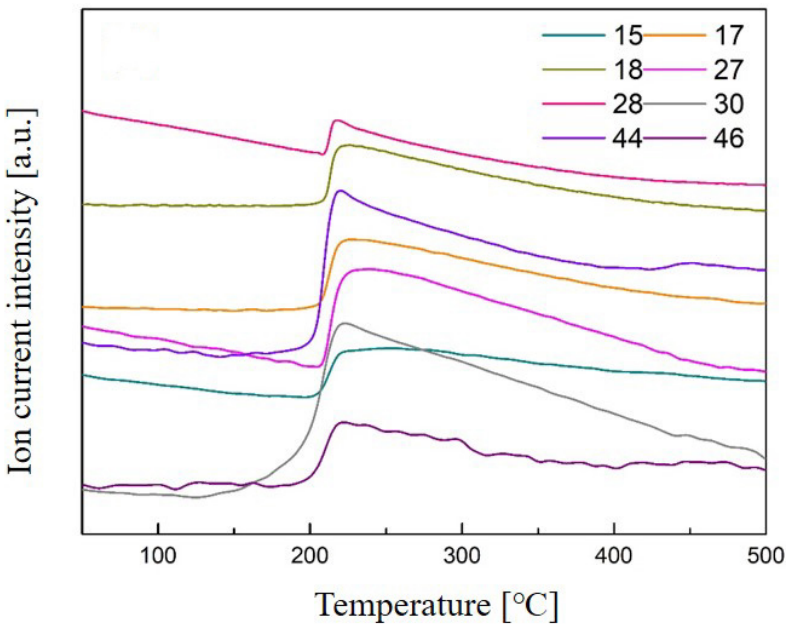

(d)

Figure 3. MS of the ion products from TKX-50 samples decomposed at 10 °C·min^{-1}: (a) TKX-50; (b) TKX-50 + $ZnFe_2O_4$, (c) TKX-50 + $CoFe_2O_4$, and (d) TKX-50 + $NiFe_2O_4$

3.3 Gas-phase FTIR analysis

The three-dimensional FTIR spectra of the gas-phase products from the thermal decomposition of TKX-50 at a heating rate of 10 °C·min^{-1} are shown in Figure 4. Figures 4(a)-4(d) show that there was no significant difference in the peak wavenumbers of the gas-phase TKX-50 decomposition products on adding the different catalysts. However, the band at 2237 cm^{-1} reached a maximum at different times, for neat TKX-50 (31.21 min), TKX-50 + $ZnFe_2O_4$ (27.82 min), TKX-50 + $CoFe_2O_4$ (27.81 min) and TKX-50 + $NiFe_2O_4$ (29.18 min), which coincides with the results from the *in-situ* FTIR and MS measurements. The gas-phase FTIR spectra of neat TKX-50 and TKX-50 mixed with $ZnFe_2O_4$, $CoFe_2O_4$ and $NiFe_2O_4$ obtained at 31.21, 27.82, 27.81 and 29.18 min are shown in Figure 4(e). The peaks at 2237, 2208, 1306 and 1270 cm^{-1} are derived from N_2O, and the bands at 2355, 2320 and 668 cm^{-1} are attributed to CO_2 from TKX-50 decomposition. Additionally, the bands at 3341, 3277 and 713 cm^{-1} are attributed to the HCN from TKX-50 decomposition. The peaks

around 3700 cm^{-1} and the peak at 2115 cm^{-1} are caused by H_2O and CO, respectively [25]. As confirmed by the results of the *in-situ* FTIR and gas-phase MS-FTIR measurements, the initial decomposition temperature of TKX-50 was clearly reduced after adding MFe_2O_4 (M = Zn, Co and Ni). Of the different catalysts, the initial decomposition temperature of TKX-50 + $CoFe_2O_4$ was decreased by the maximum degree, which also confirmed the excellent catalytic activity of $CoFe_2O_4$.

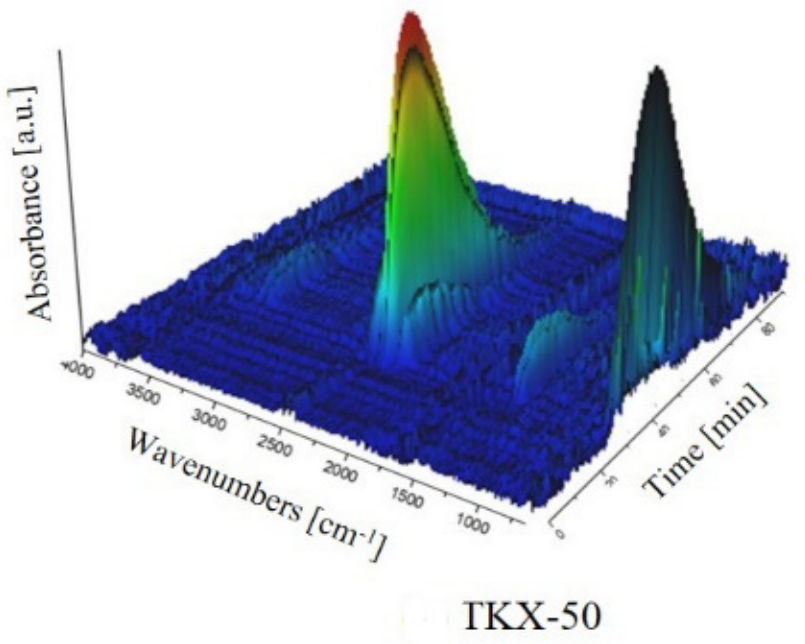

(a)

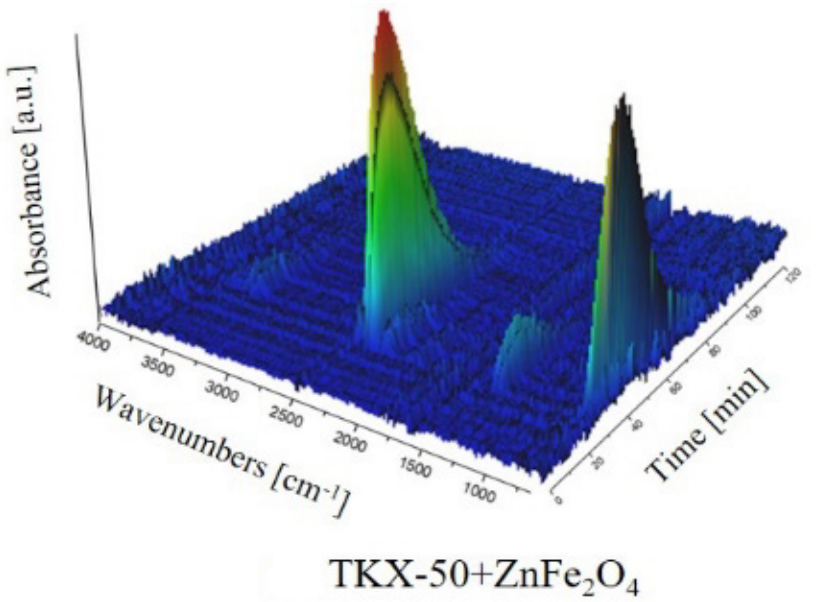

(b)

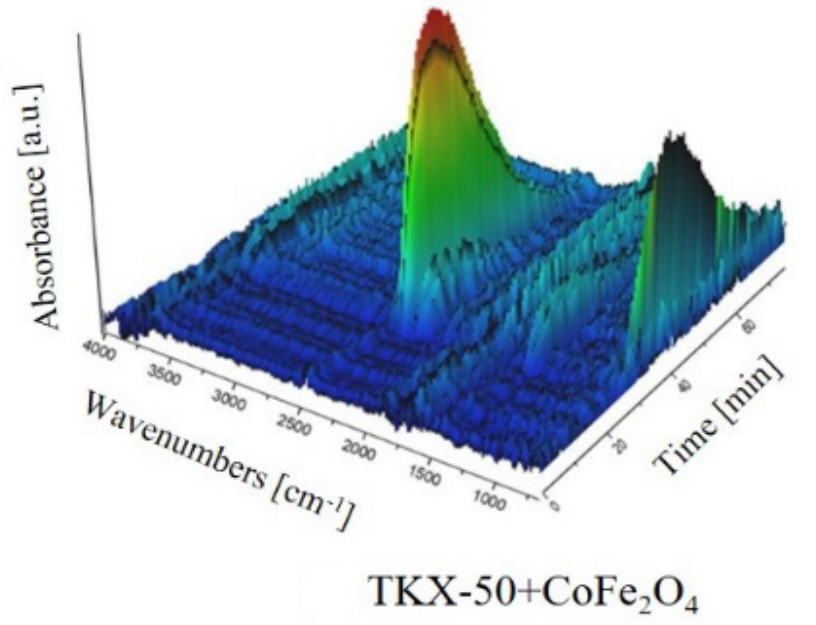

(c)

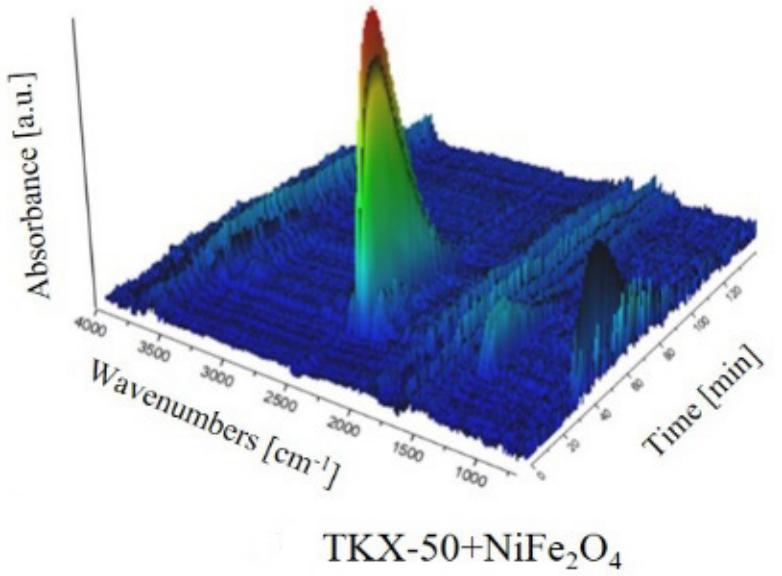

(d)

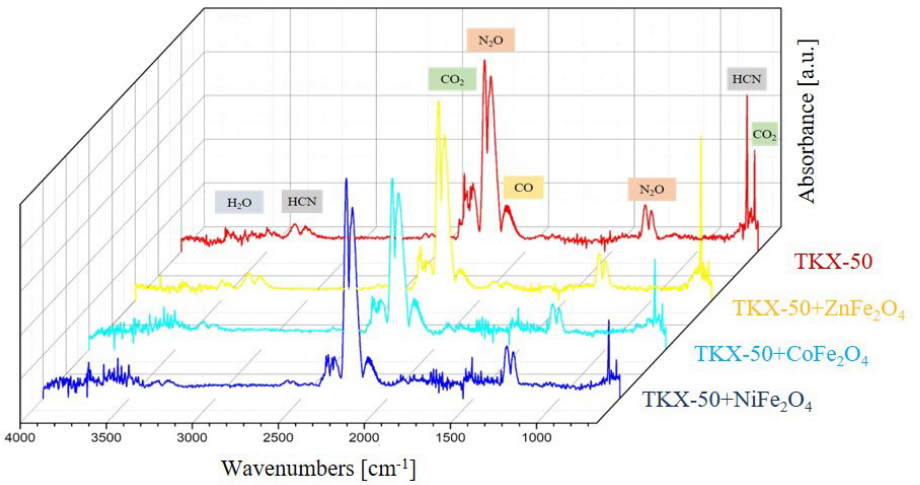

(e)

Figure 4. Three-dimensional gas-phase FTIR spectra at a heating rate of 10 °C·min^{-1} (a) TKX-50, (b) TKX-50 + $ZnFe_2O_4$, (c) TKX-50 + $CoFe_2O_4$, (d) TKX-50 + $NiFe_2O_4$, (e) gas-phase FTIR spectra of TKX-50 mixed with MFe_2O_4

3.4 Kinetic analysis of characteristic group cleavage

The conversion degree (α) of the C–C bond, N–O bond and tetrazole ring of neat TKX-50 and TKX-50 + $ZnFe_2O_4$ were calculated using the transmittance data at heating rates of 5, 10, 15 and 20 °C·min^{-1} according to Equation 1, and the corresponding curves are shown in Figure 5. Of the various mechanism functions, the $g(\alpha)$ in Equation 3 is suitable, which is consistent with previous studies. As shown in Equation 3, the decomposition of the characteristic groups is controlled by a two-dimensional diffusion mechanism, and the decomposition reaction obeys a Jander equation of $n = 1/2$. The activation energies for the characteristic groups, calculated according to Equation 2 (α = 50-85%), are listed in Table 2. For neat TKX-50, the activation energy of N–O bond cleavage is lower than the cleavage of the tetrazole ring and the C–C bond, the correlation coefficient (r) being greater than 0.98, indicating the accuracy of these results. After the addition of $ZnFe_2O_4$, the activation energies for the tetrazole ring, C–C bond and N–O bond cleavage decreased clearly, and the activation energy for the tetrazole ring was reduced to the maximum degree, demonstrating the excellent catalytic effect of $ZnFe_2O_4$ on the cleavage of the tetrazole ring.

$$g(\alpha) = [1 - (1 - \alpha)^{\frac{1}{2}}]^{\frac{1}{2}} \tag{3}$$

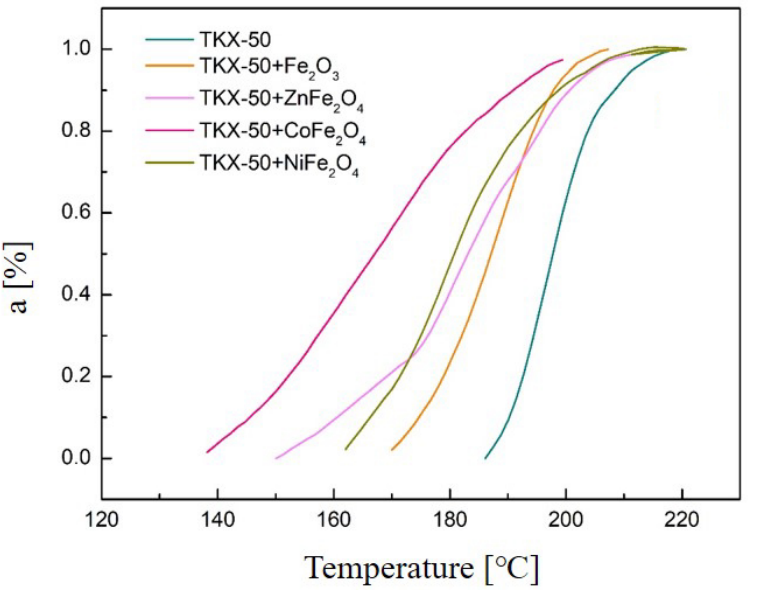

(a)

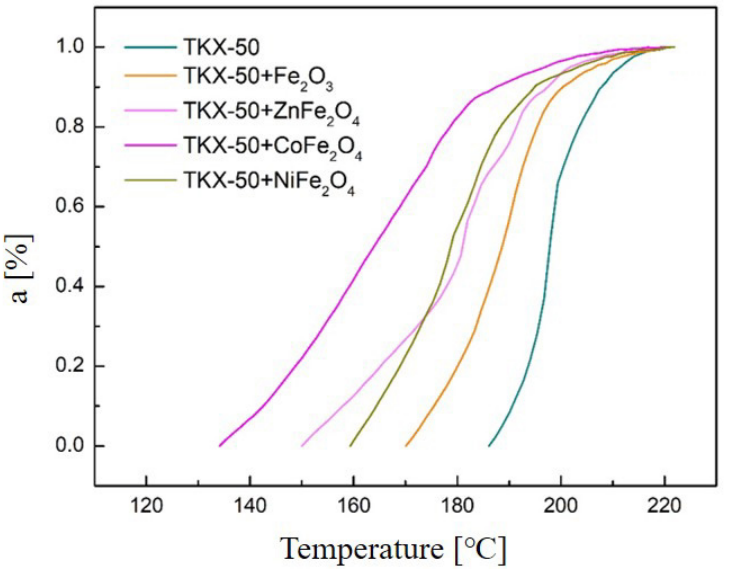

(b)

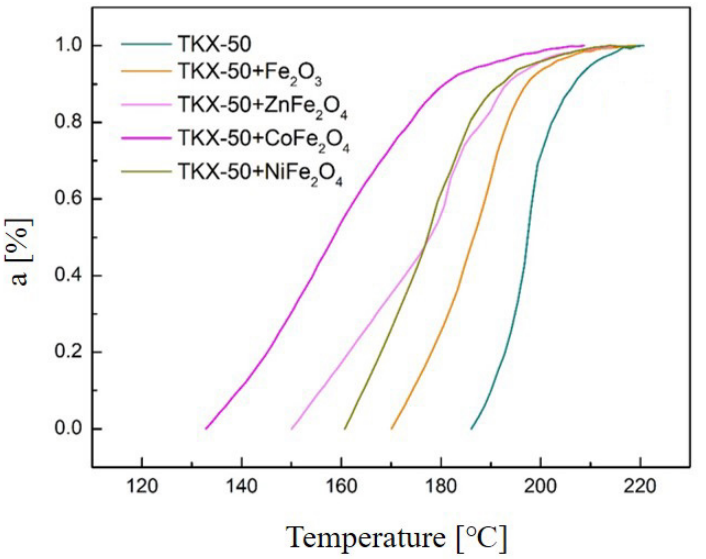

(c)

Figure 5. Conversion curves for the characteristic groups of TKX-50 before and after mixing with different catalysts: (a) C–C bond located at 719 cm^{-1}, (b) N–O bond located at 1235 cm^{-1}, (c) tetrazole ring located at 1526 cm^{-1}

Table 2. Kinetic parameters for the thermal decomposition of the characteristic groups of TKX-50 obtained by the Coats-Redfern method

Sample	Tetrazole ring		N–O bond		C–C bond	
	E_a [kcal·mol^{-1}]	r	E_a [kcal·mol^{-1}]	r	E_a [kcal·mol^{-1}]	r
TKX-50	49.7	0.992	38.7	0.998	69.7	0.997
TKX-50/ $ZnFe_2O_4$	13.0	0.988	13.9	0.991	18.9	0.995

3.5 Decomposition mechanism analysis

The decomposition mechanism of TKX-50 before and after mixing with $ZnFe_2O_4$ was analyzed based on the results of the *in-situ* FTIR and gas-phase MS-FTIR measurements. The thermal decomposition of TKX-50 can be divided into several processes, including protonation, hydroxylamine (NH_4OH) decomposition, cleavage of the tetrazole ring and the formation of stable products (shown in Figure 6). Initially, proton transfer results in the formation of 1,1'-bistetrazole diol (BTO) and hydroxylamine. Then hydroxylamine decomposes to generate the gaseous products, H_2O, NH_3 and N_2O, at a temperature below 150 °C [26]. Subsequently, the generated NH_3 reacts with BTO to form diammonium 5,5'-bistetrazole-1,1'-diolate (ABTOX), which has been confirmed by previous studies [27, 28]. Finally, BTO decomposes to N_2, NO, N_2O, HCN, HN_3, CO, CO_2 and other polymeric residues. This process corresponds to the first decomposition peak of TKX-50, accompanied by rapid heat release. The dissociation of ABTOX into BTO and NH_3 corresponds to the initial step of the second stage of TKX-50 decomposition. As in the first stage of TKX-50 decomposition, the BTO formed is decomposed into stable products [29, 30].

As is shown in Table 2 and Figure 1, the BTO formed from neat TKX-50 decomposition follows the sequence of N–O bond, tetrazole ring and C–C bond cleavage. The addition of $ZnFe_2O_4$ has an obvious effect on the thermal decomposition mechanism of TKX-50. The calculated results indicated that the $ZnFe_2O_4$ plays a significant role in the cleavage of the tetrazole ring, and obviously reduced the activation energy of tetrazole ring cleavage. As shown in Table 2, the activation energies of tetrazole ring, N–O bond and C–C bond cleavage are clearly reduced after the addition of $ZnFe_2O_4$. Besides, the cleavage order of the characteristic groups changed after the addition of $ZnFe_2O_4$ (Figure 1). In addition, the MS-FTIR results showed that the gaseous products from TKX-50 decomposition did not change significantly on mixing with the MFe_2O_4 (M = Ni, Zn, Co) samples. Therefore, the catalytic effect of MFe_2O_4 (M = Ni, Zn and Co) on the thermal decomposition of TKX-50 is mainly due to the influence

on the reaction kinetics [31]. Additionally, the reduction of the initial decomposition peak temperature confirmed the catalytic effects of MFe_2O_4 (M = Ni, Zn and Co) on TKX-50 thermal decomposition. The excellent catalytic activity of $ZnFe_2O_4$ can be attributed to the synergistic effects between Zn and Fe, which is conducive to the cleavage of the tetrazole ring of TKX-50 [32].

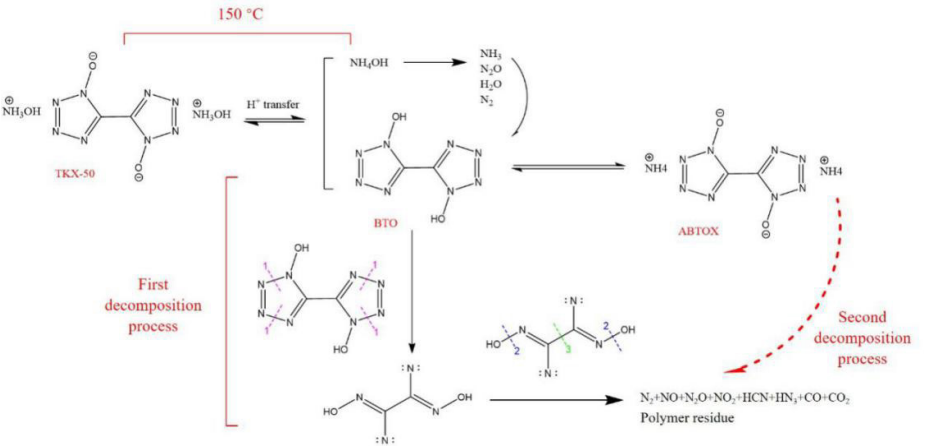

Figure 6. Proposed thermal decomposition mechanism of TKX-50 + $ZnFe_2O_4$

4 Conclusions

- The catalytic mechanisms of MFe_2O_4 (M = Ni, Co and Zn), prepared *via* a facile one-pot solvothermal method, on the thermal decomposition of TKX-50 were studied by *in-situ* FTIR and gas-phase MS-FTIR methods.
- The *in situ* FTIR and gas-phase MS results showed that the MFe_2O_4 used could effectively promote the thermal decomposition of TKX-50, and that $ZnFe_2O_4$ exhibits the best catalytic activity for TKX-50 thermal decomposition. The activation energies for the characteristic group cleavages of TKX-50, before and after mixing with multi catalysts, were calculated and used for mechanism analysis.
- The results showed that the decomposition of characteristic groups is controlled by a two-dimensional diffusion mechanism, and that the activation energies for tetrazole ring cleavage is reduced to the maximum degree by the addition of $ZnFe_2O_4$. Additionally, the addition of the catalyst has no obvious effect on the gaseous decomposition products of TKX-50.
- The excellent catalytic activity of $ZnFe_2O_4$ for TKX-50 thermal

decomposition can be attributed to the reduction of the activation energy of tetrazole ring cleavage.

Acknowledgements

Financial support by the National Natural Science Foundation of China (Grant number: 21173163) is gratefully acknowledged.

References

[1] Li, H.; Zhao, F.Q.; Gao, H.X.; Tong, J.F.; Wang, B.Z.; Zhai, L.J.; Huo, H. Three Energetic Salts Based on Oxy-bridged Bis(gem-Dinitro) Furazan: Syntheses, Structures and Thermal Behaviors. *Inorg. Chim. Acta* **2014**, *423*: 256-262.

[2] Anniyappan, M.; Sonawane, S.H.; Pawar, S.J.; Sikder, A.K. Thermal Decomposition and Kinetics of 2,4-Dinitroimidazole: An Insensitive High Explosive. *Thermochim. Acta* **2015**, *614*: 93-99.

[3] Walsh, M.R.; Thiboutot, S.; Walsh, M.E.; Ampleman, G. Controlled Expedient Disposal of Excess Gun Propellant. *J. Hazard. Mater.* **2012**, *219-220*: 89-94.

[4] Liu, L.; Li, J.; Zhang, L.; Tian, S. Effects of Magnesium-based Hydrogen Storage Materials on the Thermal Decomposition, Burning Rate, and Explosive Heat of Ammonium Perchlorate-based Composite Solid Propellant. *J. Hazard. Mater.* **2018**, *342*: 477-481.

[5] Wang, Y.L.; Zhao, F.Q.; Ji, Y.P.; Yan, Q.L.; Yi, J.H.; Xu, S.Y.; Lu, X.M. Synthesis and Thermal Behaviors of 1,8-Dihydroxy-4,5-dinitroanthraquinone Barium Salt. *J. Anal. Appl. Pyrolysis* **2014**, *105*: 295-300.

[6] Wu, Q.; Zhu, W.; Xiao, H. A New Design Strategy for High-energy Low-sensitivity Explosives: Combining Oxygen Balance Equal to Zero, a Combination of Nitro and Amino Groups, and N-Oxide in One Molecule of 1-Amino-5-nitrotetrazole-3*N*-oxide. *J. Mater. Chem. A* **2014**, *2*: 13006-13015.

[7] Li, Y.; Huang, H.; Shi, Y.; Yang, J.; Pan, R.; Lin, X. Potassium Nitraminofurazan Derivatives: Potential Green Primary Explosives with High Energy and Comparable Low Friction Sensitivities. *Chem. – Eur. J.* **2017**, *23*: 7353-7360.

[8] Zhang, X.Q.; Yuan, J.N.; Selvaraj, G.; Ji, G.F.; Chen, X.R.; Wei, D.Q. Towards the Low-sensitive and High-energetic Co-Crystal Explosive CL-20/TNT: from Intermolecular Interactions to Structures and Properties. *Phys. Chem. Chem. Phys.* **2018**, *20*: 17253-17261.

[9] Sinditskii, V.P.; Filatov, S.A.; Kolesov, V.I.; Kapranov, K.O.; Asachenko, A.F.; Nechaev, M.S.; Shishov, N.I. Combustion Behavior and Physico-Chemical Properties of Dihydroxylammonium 5,5′-Bistetrazole-1,1′-diolate (TKX-50). *Thermochim. Acta* **2015**, *614*: 85-92.

[10] Didier, M. Sensitivity of Energetic Materials: Theoretical Relationships to Detonation Performance and Molecular Structure. *Ind. Eng. Chem. Res.* **2017**, *56*:

8191-8201.

[11] An, Q.; Cheng, T.; Goddard, W.A.; Zybin, S.V. Anisotropic Impact Sensitivity and Shock Induced Plasticity of TKX-50 (Dihydroxylammonium 5,5′-Bis(tetrazole)-1,1′-diolate) Single Crystals: From Large-Scale Molecular Dynamics Simulations. *J. Phys. Chem. C* **2015**, *119*: 2196-2207.

[12] Wang, Y.; Zhu, J.; Yang, X.; Lu, L.; Wang, X. Preparation of NiO Nanoparticles and Their Catalytic Activity in the Thermal Decomposition of Ammonium Perchlorate. *Thermochim. Acta* **2005**, *437*: 106-109.

[13] Yan, Q.L.; Liu, L.L.; He, W.; Luo, C.; Shlomovich, A.; Liu, P.-J.; Gozin, M. Decomposition Kinetics and Thermolysis Products Analyses of Energetic Diaminotriazole-substituted Tetrazine Structures. *Thermochim. Acta* **2018**, *667*: 19-26.

[14] Wang, J.; Ma, X.; Yu, Z.; Peng, X.; Lin, Y. Studies on Thermal Decomposition Behaviors of Demineralized Low-lipid Microalgae by TG-FTIR. *Thermochim. Acta* **2018**, *660*: 101-109.

[15] Huang, H.; Shi, Y.; Yang, J. Thermal Characterization of the Promising Energetic Material TKX-50. *J. Therm. Anal. Calorim.* **2015**, *121*: 705-709.

[16] Jia, J.; Liu, Y.; Huang, S.; Xu, J.; Li, S.; Zhang, H.; Cao, X. Crystal Structure Transformation and Step-by-Step Thermal Decomposition Behavior of Dihydroxylammonium 5,5′-Bistetrazole-1,1′-diolate. *RSC Adv.* **2017**, *7*: 49105-49113.

[17] Muravyev, N.V.; Monogarov, K.A.; Asachenko, A.F.; Nechaev, M.S.; Ananyev, I.V.; Fomenkov, I.V.; Pivkina, A.N. Pursuing Reliable Thermal Analysis Techniques for Energetic Materials: Decomposition Kinetics and Thermal Stability of Dihydroxylammonium 5,5′-Bistetrazole-1,1′-diolate (TKX-50). *Phys. Chem. Chem. Phys.* **2017**, *19*: 436-449.

[18] Yi, J.H.; Zhao, F.Q.; Hong, W.L.; Xu, S.Y.; Hu, R.Z.; Chen, Z.Q.; Zhang, L.Y. Effects of Bi-NTO Complex on Thermal Behaviors, Nonisothermal Reaction Kinetics and Burning Rates of NG/TEGDN/NC Propellant. *J. Hazard. Mater.* **2010**, *176*: 257-261.

[19] Ming Zhang, M.; Zhao, F.; Wang, Y.; Chen, X.; Pei, Q.; Xu, H.; Hao, H.; Yang, Y.; Li, H. Evaluation of Graphene-Ferrocene Nanocomposite as Multifunctional Combustion Catalyst in AP-HTPB Propellant. *Fuel* **2021**, 302, paper 121229: 1-9.

[20] Zhang, M.; Zhao, F.; Yang, Y.; Li, H.; Gao, H.; Yao, E.; Zhang, J.; An, T.; Jiang, Z. Synthesis, Characterization and Catalytic Behavior of MFe_2O_4 (M = Ni, Zn and Co) Nanoparticles on the Thermal Decomposition of TKX-50. *J. Therm. Anal. Calorim.* **2020**, *141*: 1413-1423.

[21] Zhang, M.; Zhao, F.; Yang, Y.; An, T.; Qu, W.; Li, H.; Zhang, J.; Li, N. Catalytic Activity of Ferrates ($NiFe_2O_4$, $ZnFe_2O_4$ and $CoFe_2O_4$) on the Thermal Decomposition of Ammonium Perchlorate. *Propellants Explos., Pyrotech.* **2020**, *45*: 463-471.

[22] Zhang, M.; Zhao, F.; Yang, Y.; Li, H.; Zhang, J.; Ma, W.; Gao, H.; Li, N. Shape-Dependent Catalytic Activity of Nano-Fe_2O_3 on the Thermal Decomposition of TKX-50. (in Chinese) *Acta Phys.-Chim. Sin.* **2020**, *36*, paper 1904027.

[23] Zhang, M.; Zhao, F.; Yang, Y.; Zhang, J.; Li, N.; Gao, H. Effect of rGO-Fe_2O_3 Nanocomposites Fabricated in Different Solvents on the Thermal Decomposition Properties of Ammonium Perchlorate. *CrystEngComm* **2018**, *20*: 7010-7019.
[24] Vovk, E.I.; Turksoy, A.; Bukhtiyarov, V.I.; Ozensoy, E. Interactive Surface Chemistry of CO_2 and NO_2 on Metal Oxide Surfaces: Competition for Catalytic Adsorption Sites and Reactivity. *J. Phys. Chem. C* **2013**, *117*: 7713-7720.
[25] Singh, S.; Wu, C.; Williams, P.T. Pyrolysis of Waste Materials using TGA-MS and TGA-FTIR as Complementary Characterisation Techniques. *J. Anal. Appl. Pyrolysis* **2012**, *94*: 99-107.
[26] Wang, J.; Chen, S.; Jin, S.; Shi, R.; Yu, Z.; Su, Q.; Shu, Q. The Primary Decomposition Product of TKX-50 under Adiabatic Condition and Its Thermal Decomposition. *J. Therm. Anal. Calorim.* **2018**, *134*: 2049-2055.
[27] Wang, J.; Chen, S.; Yao, Q.; Jin, S.; Zhao, S.; Yu, Z.; Shu, Q. Preparation, Characterization, Thermal Evaluation and Sensitivities of TKX-50/GO Composite. *Propellants, Explos., Pyrotech.* **2017**, *42*: 1104-1110.
[28] Zhang, M.; Zhao, F.; Yang, Y.; Li, H.; An, T.; Zhang, J. The Effect of rGO-Fe_2O_3 Nanocomposites with Spherical, Hollow and Fusiform Microstructures on the Thermal Decomposition of TKX-50. *J. Phys. Chem. Solids* **2021**, *153*, paper 109982: 1-7.
[29] Zhang, M.; Zhao, F.; Li, H.; Yang, Y.; An, T.; Jiang, Y.; Li, N. Morphology-dependent Catalytic Activity of Fe_2O_3 and its Graphene-based Nanocomposites on the Thermal Decomposition of AP. *FirePhysChem* **2021**, *1*: 46-53.
[30] Huang, H.; Shi, Y.; Yang, J. Thermal Characterization of the Promising Energetic Material TKX-50. *J. Therm. Anal. Calorim.* **2015**, *121*: 705-709.
[31] García Rodenas, L.A.; Blesa, M.A.; Morando, P.J. Reactivity of Metal Oxides: Thermal and Photochemical Dissolution of MO and MFe_2O_4 (M = Ni, Co, Zn). *J. Solid State Chem.* **2008**, *181*: 2350-2358.
[32] Chen, S.; Zhang, H.; Wu, L.; Zhao, Y.; Huang, C.; Ge, M.; Liu, Z. Controllable Synthesis of Supported Cu–M (M = Pt, Pd, Ru, Rh) Bimetal Nanocatalysts and Their Catalytic Performances. *J. Mater. Chem.* **2012**, *22*: 9117-9122.

Received: December 26, 2020
Revised: June 23, 2021
First published online: June 30, 2021